How non-bonding domains affect the active assembly of microtubule spools

Journal:	*Nanoscale*
Manuscript ID	NR-ART-03-2019-002059.R2
Article Type:	Paper
Date Submitted by the Author:	28-May-2019
Complete List of Authors:	Martinez, Haneen; Sandia National Laboratories, Center for Intergated Nanotechnologies VanDelinder, Virginia; Sandia National Laboratories, Center for Intergated Nanotechnologies Imam, Zachary; Sandia National Laboratories, Center for Intergated Nanotechnologies Spoerke, Erik; Sandia National Laboratories, Electronic, Optical, & Nano Materials Bachand, George; Sandia National Laboratories, Center for Integrated Nanotechnologies

SCHOLARONE™
Manuscripts

Nanoscale

ARTICLE

How non-bonding domains affect the active assembly of microtubule spools

Haneen Martinez, [a] Virginia VanDelinder, [a] Zachary Imam, [a] Erik D. Spoerke,[b] and George D. Bachand *[a]

Structural defects can determine and influence various properties of materials, and many technologies rely on the manipulation of defects (e.g., semiconductor industries). In biological systems, management of defects/errors (e.g. DNA repair) is critical to an organism's a survival, which has inspired the design of artificial nanomachines that mimic nature's ability to detect defects and repair damage. Biological motors have captured considerable attention in developing such capabilities due to their ability to convert energy into directed motion in reponse to environmental stimuli, which maximizes their ability for detection and repair. The objective of the present study was to develop an understanding of how the presence of non-bonding domains, here considered as a "defect," in microtubule (MT) building blocks affect the kinesin-driven, active assembly of MT spools. The assembly/joining of micron-scale bonding (i.e., biotin-containing) and non-bonding (i.e., no biotin) MTs resulted in segmented MT building blocks consisting of alternating bonding and non-bonding domains. Here, the introduction of these MT building blocks into a kinesin gliding motility assay along with streptavidin-coated quantum dots resulted in the active assembly of spools with altered morphology but retained functionality. Moreover, it was noted that non-bonding domains were autonomously and preferentially released from the spools over time, representing a mechanism by which defects may be removed from these structures. Overall, our findings demonstrate that this active assembly system has an intrinsic ability for quality control, which can be potentially expanded to a wide range of applications such as self-regulation and healing of active materials.

Introduction

Defects represent disruptions or interruptions of order, structure, or homogeneity in a material. They are found in nearly all materials to varying extents, and the nature and behaviour of defects can dramatically impact materials properties and performance. For example, n-type and p-type dopant "defects" in silicon semiconductors provide the critical electronic properties fundamental to modern microelectronics.[1,2] Oxygen defects in ceramic oxides impact ion transport properties key to solid oxide fuel cells.[3] Inclusions can degrade optical properties in glasses, while metallic dopants in alumina give rubies their vibrant color.[4] Dislocation densities and metal carbide inclusions in steel can drastically affect their strength and robustness, which is why annealing and hot working (e.g., forging) is used redistribute, segregate, or remove defects and impurities from metals.[5] Although the influence and dynamic behaviour of defects is often considered in these types of structural and technological materials, relatively little attention has been given to defects in bio-inspired supramolecular materials.

Biological organisms have evolved into highly-optimized functional systems, displaying remarkable abilities such as self-regulation and self-repair in the presence of defects or damage, further increasing the organism's lifetime. Such tasks require the cells to respond to stimuli in their environment, and most importantly, to convert chemical energy into mechanical work.[6–9] In the cell, kinesin motors harness the energy from ATP hydrolysis to actively transport intracellular components

(e.g., vesicles, chromosomes) along cytoskeletal networks composed of microtubule (MT) filaments, with high efficiency (~50%).[10–14] Inspired by their cellular function, researchers have been inspired to develop nanomachines capable of mimicking and/or co-opting biological materials for the development of dynamic, synthetic materials.[15,16] Because biomolecular motors offer the ability to respond to different environmental stimuli through their regulated collective movement, they are of prime interest as a template in developing nanomachines that could sense defects and repair damage.[9,17–22] Other researchers have sidestepped the challenge of creating synthetic nanomachines by using kinesin motors for *ex vivo* applications such as powering analytical, diagnostic, and computational devices,[23–26] and active assembling nanostructured, non-equilibrium materials.[10,25,27,28]

To date, the possibility of using kinesin motors to repair defects in *ex vivo* materials has not been explored. MTs are able to self-repair mechanically induced defects in the tubulin lattice through the incorporation of tubulin subunits from solution.[29–31] Although this ability demonstrates the robustness of the MTs *ex vivo*, much less is known about the formation and effects of defects in supramolecular structures and composites assembled with the kinesin-MT transport system. One example of such a system involves the active assembly of rings and spools, where a ring is defined as single filament or filament bundle that cross-links to itself to form a closed loop, and a spool is composed of many crosslinked filaments.[27,28,32–35] In this system, biotinylated MTs serve as the fundamental building blocks, and the binding of streptavidin or streptavidin-coated quantum dots (sQDs) drives their spontaneous assembly into rings and spools. While serving as an interesting model of active assembly, the formation of rings and spools may also be used as a sensing element. For example, label-free detection of microvesicles was recently reported based on the formation of spools.[36]

While fluorescent microscopy suggests that the spools are relatively well-ordered, electron microscopy reveals that these structures are topographically and morphologically diverse including twisted and kinked domains, as well as in-plane and out-of-plane loops.[37,38] These observations suggest spools can tolerate a certain level of structural heterogeneity, but the question remains as to whether they can compensate for MT building blocks that have large (e.g., micron-scale) domains that lack biotin and are unable to bind sQDs. The large number of biotin-streptavidin bonds that are formed among MTs and sQDs during assembly is critical to stabilizing the high bending energy (~30,000 kT per turn) stored in these structures.[38–40] As such, the tolerance of assembly and the resulting spools should be strongly dependent on the relative size and frequency of the domains that lack biotinylated tubulin.

To test this hypothesis, we characterized the active assembly of spools using MT building blocks composed of varying lengths and frequency of "bonding" and "non-bonding" domains. Herein, we define bonding domains and MTs as those containing biotinylated tubulin and therefore "compliant" in their ability to form biotin-streptavidin bonds. In contrast, non-bonding domains and MTs are defined as those polymerized in the absence of biotinylated tubulin and thus represent "defects" due to their inability to form biotin-streptavidin bonds. The process goal was to determine whether "pure" spools of bonding domains and sQDs (target cargo) could be obtained through kinesin-driven assembly of the segmented MTs. Using these MT building blocks, we observed the incorporation of bonding and non-bonding domains and MTs into spools, but also the autonomous and preferential removal of non-bonding domains and MTs from spools over time. We hypothesize that this phenomenon is related to the inability of these domains and MTs to balance high bending energy with covalent bond formation, as well as mechanical strain due to mismatches in kinesin motor velocities. Overall, this work provides new insights into the influence and behaviour of defective building blocks in dynamic supramolecular materials that may have important implications for the future engineering of self-regulating and self-healing nanomaterials.

Results and discussion

The relative ratio of biotinylated (i.e. bonding) tubulin and sQDs regulates the active self-assembly of spools; bonding MTs will form spools at concentrations of biotinylated tubulin as low as 10%,[40] ~160 biotinylated dimers per micron. Consequently, bonding MTs will have small regions lacking biotinylated tubulin (i.e., tens of nm); these regions, however, have a negligible effect on the structure and function of the spools. To more fully understand how MT structure affects assembly of the spools, we formed segmented MT building blocks through the directed self-assembly (i.e., joining) of varying ratios of bonding and non-bonding MTs[31,41,42].

Two populations of MTs were independently polymerized and subsequently combined together to form segmented MTs with varying levels of bonding and non-bonding domains (Fig. 1a). Bonding MTs (blue) were formed by polymerizing unlabeled, biotinylated, and aminomethylcoumarin (AMCA)-labeled tubulin; non-bonding MTs (green) by polymerizing unlabeled and HiLyte® 488-labeled tubulin. Directed self-assembly yielded segmented MTs with alternating bonding

(blue) and non-bonding (green) domains (Fig. 1b) of varying sizes and frequency. The average lengths and number of bonding and non-bonding domains in the different segmented
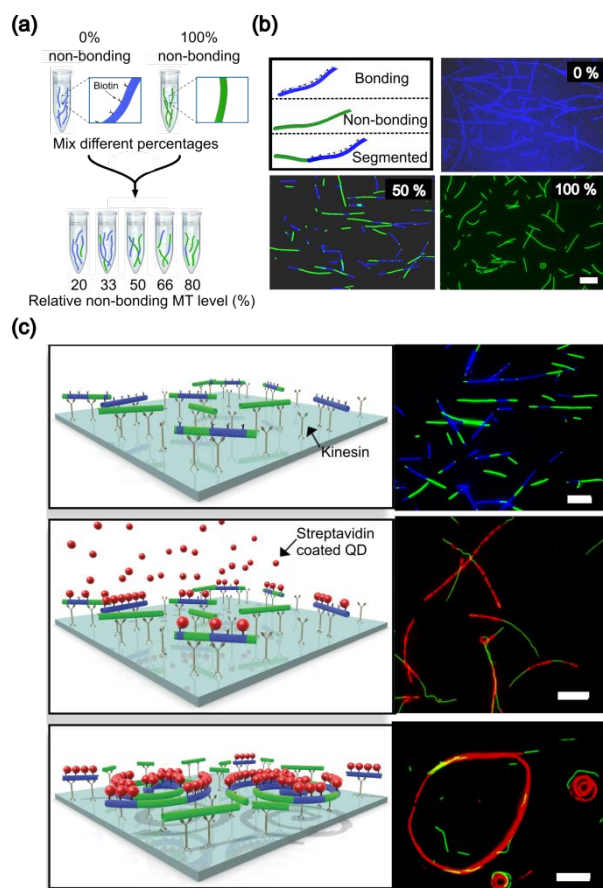
Fig. 1. Assembly of spools using segmented MTs. (a) Formation of segmented MTs by mixing various ratios of bonding (blue) and non-bonding (green) MTs. (b) Photomicrographs showing the resulting three types of MTs: blue, bonding MTs, green, non-bonding MTs, and blue-green segmented MTs consisting of bonding and non-bonding domains. (c) Schematic illustration of the gliding motility assay used to assemble the spools in which surface-bound kinesins translate the MTs (top panel); the addition of streptavidin-coated QDs (middle panel) results in the formation of spools (bottom panel). Scale bars = 10 μm.

MTs is shown in Fig. S2. The resulting MTs were introduced into the gliding motility assay (Fig. 1c, top), followed by the introduction of sQDs (Fig. 1c, middle and bottom) to initiate the active assembly of spools, which were characterized by fluorescence microscopy.

The morphology of the spools revealed qualitative changes based on the introduction of MTs containing non-bonding domains. When only bonding MTs (control) were present, the

resulting spools generally adopted an ovular or circular shape with densely packed MT layers and occasional structural variants in the form of loops and spirals (Fig. 2a, 0%), consistent with prior reports.[33,38,43,44] With segmented MTs, the spools adopted more irregular shapes characterized by a decrease in the packing MT density, as well as larger gaps and loops that were primarily associated with non-bonding domains (Fig. 2a). Unbound 'tails' consisting of non-bonding (green) domains of the segmented MTs was commonly observed (Fig. 2a). Overall these observations demonstrate the ability of kinesin motors to drive the assembly of stable, albeit morphologically altered, spools from segmented MT building blocks.

We assessed the quantitative differences between the bonding and segmented spools by measuring the inner diameter of MT spools, which has been shown to reflect the nucleation mechanism.[32] The average inner diameters (Fig. S1a) formed from bonding (0%) and segmented (20-80%) MTs were similar, 2.3 ± 2.2 μm (mean ± standard deviation) and 2.1 ± 1.5 μm, respectively ($P = 0.481$), suggesting that spools formed from
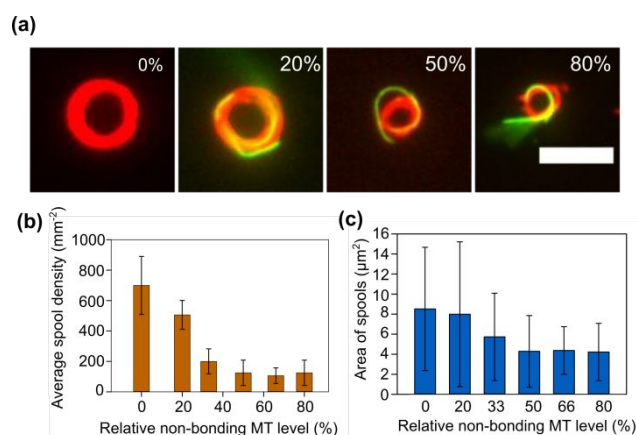
Fig. 2. Spool morphology and size. (a) Fluorescence micrographs of spools showing structural differences across the different percentages of non-bonding MT domains. Scale bar = 5 μm. Average (b) density and (c) area of spool for different levels of non-bonding MTs. Error bars = standard deviation. Number of measurements (n) used to determine spool density was 10 fields of view for each treatment; n used to determine spool areas was 98, 101, 44, 29, 20, and 26 for 0, 20, 33, 50, 66, and 80% non-bonding domains, respectively.

both types of building blocks assembled by a combination of pinning and simultaneous collision.[32] The density of spools (i.e., number of spools per area) was also evaluated at 30 min post-introduction of sQDs. Here, a significant decrease in the density of spools was observed when comparing bonding (0%) and segmented (20-80%) MTs, 700 ± 190 and 213 ± 79 mm^{-2},

respectively ($P < 0.001$). Further, the density of spools exhibited an inverse correlation with respect to percentage of non-bonding domains (Fig. 2b; $r = -0.895$; $P = 0.02$), which intuitively may be explained by the reduction in bonding domains capable of nucleating the formation of a spool.
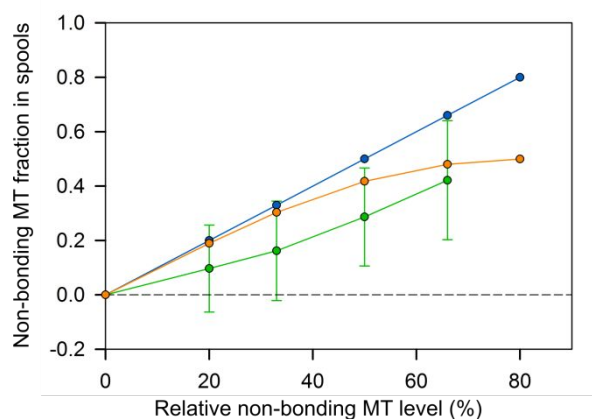
Fig. 3. Theoretical vs. measured fraction of non-bonding MTs in spools. The blue line shows the fraction of non-bonding MTs that would theoretically be expected in spools assuming that all types of MT building blocks were incorporated at an equivalent rate. The orange line extends this theory with the assumption that only bonding and segmented MTs are incorporated into spools. Here, measured experimental data of the initial MT counts and length distributions were used in the theory to predict the fraction in spools. The green line shows the measured fraction of non-bonding MTs in spools based on fluorescence images. Error bars = standard deviation. Note: (80% defects data excluded due to insufficient number of observations and large variability).

The subsequent growth of the spools may be characterized by the thickness and/or area of a spool. These properties are a product of (*i*) the growth process in which colliding MTs are sequentially added to the outer perimeter of the existing spools,[38,45] and (*ii*) the loss of any MTs from the rotating spools. The average thickness of spools (Fig. S1b) formed by segmented MTs (0.6 ± 0.3 μm) was significantly smaller than those formed by bonding MTs (0.9 ± 0.4 μm; $P < 0.01$). Further, the thickness of the spools was inversely correlated to the percentage of non-bonding domains and MTs (Fig. S1b; $r = -0.973$; $P < 0.002$). The mean area of a spool formed from segmented MTs (6.3 ± 5.8 μm^2) was also significantly smaller than that observed for bonding MTs (8.5 ± 6.2 μm^2; $P < 0.001$), and inversely correlated with the percent of non-bonding domains and MTs (Fig. 2c; $r = -0.925$; $P = 0.008$). Collectively these results suggest that the presence of non-bonding MTs has adverse effect on the growth of spools.

Examing the fraction of non-bonding domains and MTs in spools can offer important insights as to how domains that cannot form biotin-streptavidin bonds are managed during the assembly and growth processes. If one assumes that all MTs are incorporated at equivalent rates, the fraction non-bonding domains and MTs expected to be incorporated into spools may be estimated simply by the ratio of the two different MT types (Fig. 3, blue line). Because non-bonding MTs lack biotin, it is assumed that their incorporation into spools should be minimal and may be removed from the theory by excluding purely non-bonding MTs (Fig. 3, orange line). Here, measured experimental values of the number and lengths of non-bonding MTs (Fig. S2) were used in the modified theory. These estimates were then directly compared with experimental data in which the fraction of non-bonding MTs in spools was measured via fluorescent intensity at 30 min, (green line; note that data for 80% defects were excluded due to a low number of observations and high variability). Details of these calculations are provided below in the Experimental section. The measured fraction of non-bonding MT in the spools (green line) shows considerable deviation from both the theoretical predictions (blue and orange lines), which may be explained by two potential mechanisms. First, although the segmented MTs can incorporate into spools, the frequency of incorporation may be lower due to the presence of non-bonding domains. Alternatively, the non-bonding domains of the segmented MTs that were initially incorporated into the spools may be broken and released due to the high bending energy in the spool and inability of non-bonding domains to compensate for this energy with stabilizing biotin-streptavidin bonds. In addition, because spools rotate at a constant angular velocity, the kinesin motors transport MTs at different linear velocities depending on where they are in the spool,[40] which can lead to additional strain between adjacent MTs in a spool. The latter hypothesis (i.e., removal of non-bonding domains) is exemplified in Fig. 4a, where a non-bonding tail is severed from a spool. As these tails are not stabilized through lateral bonding to adjacent MTs, sharp kinks and bends may form as the spool rotates; during such events, the tail segment forms a bend that exceeds the critical radius of curvature (~0.6 μm)[46] at which point the non-bonding domains of the segmented MTs break, and are released from the spool. This behavior is a direct result of the dynamic character of this motor-driven, non-equilibrium system.

Breakage and release of the non-bonding domains of the segmented MTs over time should result in an overall increase in the number of non-bonding MTs moving freely in the gliding motility assay (i.e., green MTs not associated with spools). Thus, the release of non-bonding domains of the segmented

(a)

(b)
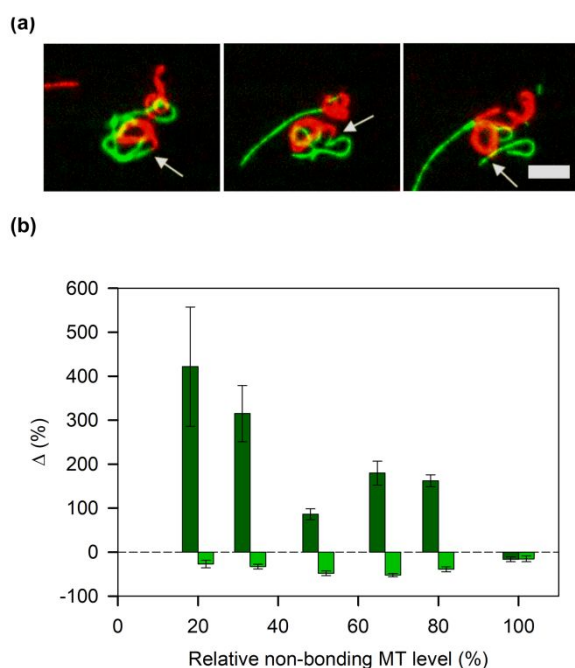
Fig. 4. Breakage and release of non-bonding MTs. (a) Time-lapse micrographs demonstrating breakage and release of a non-bonding domain. Scale bar = 5 μm. (b) Change in average density (■) and average length (■) of free non-bonding MTs as a function of the relative non-bonding MT level (t= 30 min). Number of measurements (*n*) used are listed in Fig. S4 & S5. Error bars = propagated standard errors.

(a)

(b)

(c)

(d)

Fig. 5. Spools integrate or reject MTs upon collision. Time-lapse micrographs showing (a) rejection of bonding MT (red), and (b) integration of non-bonding MT (green) into the spool. Note: the spool is rotating counter-clockwise. Scale bar = 5 μm. (c,d) Collision angles of free non-bonding (●),bonding(●), and segmented (●) MTs that integrated into (outer) or were rejected from (inner) spools. d) diagrams of a MT encountering spools at angle θ greater than (left) and less than (right) 90˚.

MTs may be quantified by measuring the density of free green MTs at various time points (Fig. S3a). Indeed, we observed an average increase of ~190% in the number of non-bonding MTs across the different non-bonding levels (20-80%) over a thirty-minute period. As shown in Fig. 4b, this effect was dependent upon the ratio of non-bonding in segmented MTs, with the greatest increase in density of free non-bonding MTs was observed at 20% defects (421% increase), and the smallest increase was observed at 50% defects (86% increase). These data support the hypothesis that segmented MTs are preferentially broken into bonding and non-bonding MTs, and that the non-bonding MTs are disproportionately released from the spools due to the lack of stabilizing biotin-streptavidin bonds. To ensure that the observed increase was not simply caused by random shearing or breakage of MTs, we also quantified the change in length of non-bonding MTs over the same period (Fig. 4b and S3b). Here, a ~36% decrease in length was observed for non-bonding MTs (20-80% defect levels). It is likely that non-bonding domains removed from spools

experience shortening, as the breakage that releases these domains will not occur solely at the interface of non-bonding and bonding domains, but also in the middle of non-bonding domains. The change in density and length of bonding and segmented MTs was also measured to confirm that the release of non-bonding MTs was indeed preferential, relative to the bonding MTs. These data suggest that bonding and segmented MTs are released from spools, but at a much lower level (Fig. S4 and S5). Thus, we conclude that defect, non-bonding domains and MTs are autonomously and preferentially removed as part of the active self-assembly of MT spools.

We also assessed how non-bonding domains and MTs affected the incorporation of MT building blocks during spool growth. Fig. 5a shows an example of a bonding MT being rejected from a spool, while Fig. 5b shows a non-bonding MT being incorporated into the same spool. We observed that the collision angle (θ) determined whether an MT building block would either be incorporated into or rejected by the growing spool. Specifically, MTs colliding with rotating spools displayed a significantly greater probability of being incorporated when θ < 90° (P < 0.0001; Fig. 5c, d). Incorporation was independent of the MT type; i.e., all three MT types displayed similar rates of incorporation at θ < 90°. While this observation may appear inconsistent with regard to non-bonding MTs, the incorporation of non-bonding MTs into spools is transient and likely results from being sterically trapped in gaps/loops in the spool. Collisions at θ > 90° largely result in rejection of the MT building blocks due to the shear force generated by MTs moving in opposing directions.

By segregating and eliminating the non-bonding defective domains of the segmented MTs, the energy dissipated during assembly effectively parallels the action of defect annealing and hot-working in metals, where thermal or mechanical energy are used to redistribute or remove defective domains from a material. In effect, the active assembly process is prioritizing functionality, and eliminating MTs that fail to meet the functional standard of this system. Collectively, this knowledge establishes a critical foundation upon which more advanced biomolecular and hybrid nanomaterials may be designed and developed based on active assembly processes.

Conclusions

Here, we described how defect, non-bonding domains in MT building blocks affect the active assembly and behaviour of motor-driven MT spools. Active assembly of spools was observed using segmented MT building blocks consisting of alternating bonding (biotinylated) and non-bonding domains with varying lengths and frequencies. Use of these building blocks resulted in spools with altered morphologies, reduced densities, and reduced areas. Moreover, we observed the autonomous and preferential removal of the non-bonding domains from spools over time, which may be attributed to the lack of bond formation necessary to offset the mechanical strain induced during the dynamic rotation of the spools. Furthermore, the ability of free MTs (segmented, bonding, and non-bonding) to incorporate into the spools was shown to be strongly contingent on the collision angle ($\theta < 90°$). Overall, our findings provide fundamental insights into how energy dissipation can be used to regulate the composition of actively assembled structures, particularly with respect to quality control from defective building blocks. Additional characterization of this system (e.g., cryo-electron microscopy) may provide further understanding with respect to the mechanism by which domains are released from spools. These observations will guide future development of nanostructured materials with adaptive and self-healing behaviours.

Experimental

Materials

Lyophilized unlabeled tubulin, Hilyte Fluor 488 (Hilyte 488) labeled tubulin, aminomethyl coumarin acetate (AMCA) labeled tubulin, and biotin labeled tubulin purified from porcine brain were purchased from Cytoskeleton Inc. (Denver, CO) and used according to manufacturer's instructions without further modification or purification. Streptavidin conjugated quantum dots (sQDs, 655nm) were purchased from ThermoFisher Scientific (Waltham, MA). All chemicals were purchased from Sigma Aldrich unless otherwise noted.

Preparation of motor proteins

Full-length *Drosophila melanogaster* kinesin-1 from the pPK113 expression plasmid was expressed in *Escherichia coli* BL21 (DE3) pLysS cells.[47] Briefly, when the culture reached an OD_{600nm} of ~0.7, protein expression was induced through the addition of 0.5 mM isopropylthio-β-galactoside (IPTG). Cells were harvested by centrifugation at 9000×g, and lysed using BugBuster® with Benzonase® (EMD Biosciences, Inc., Billerica, MA) and 100 mM AEBSF (4-(2-Aminoethyl) benzenesulfonyl fluoride hydrochloride (Sigma-Aldrich Inc., St. Louis, MO). Kinesin was then purified by Ni-NTA chromatography as previously described.[47] Protein concentration was determined by standard bicinchoninic (BCA) assay to be 4 µM. Aliquots of the protein were snap frozen in liquid nitrogen and stored at -80°C.

Preparation of Microtubules

Fluorescent, biotinylated, and unlabeled MTs were prepared by resuspending lyophilized tubulin in BRB80 buffer (80 mM PIPES pH 6.9, 1 mM $MgCl_2$,1 mM EGTA) containing 1 mM GTP and 10% glycerol to a final tubulin concentration of 5 mg ml^{-1}. AMCA labeled tubulin was combined with biotinylated and unlabeled tubulin at a molar ratio of 1:1:2, respectively, for both experimental and control population of 0% defects. Hilyte 488 tubulin and unlabeled tubulin were mixed at a molar ratio of 1:1 for experimental and control population of 100% defects. MTs were polymerized at 37°C for 30 min and stabilized against depolymerization using BRB80 solution containing 10 µM paclitaxel for a final tubulin concentration of 0.1 mg ml^{-1}. Segmented MTs were achieved by mixing biotinylated AMCA MTs with Hilyte 488 MTs at the following non-bonding percentages: 20, 33, 50, 66, and 80%. All populations mixed at different percentages, as well as the control population were incubated at room temperature for two days to allow for sufficient joining of the domains into segmented MTs.

Motility assays

Inverted kinesin motility assays were performed by constructing a capillary flow cell on a glass slide using double-sided tape and a coverslip, with average channel dimension of ~20 mm long, 5 mm wide, and 0.2 mm deep. Kinesin was diluted to 8 nM in 80mM PIPES with 2 mg mL^{-1} casein and 2 mM adenosine 5′-(β,γ-imido) triphosphate (AMP-PNP), a

nonhydrolyzable form of ATP used to immobilize the MTs. This solution was added to the flow chamber and incubated for 5 minutes. The flow cell was then washed using motility solution (BRB80 containing 0.2 mg mL^{-1} casein, 1 mM AMP-PNP, 0.02 mg mL^{-1} glucose oxidase, 0.008 mg mL^{-1} catalase, 20 mM D-glucose, and 1 mM DTT) to remove unbound motors. Paclitaxel stabilized MTs diluted in motility solution were infused into the flow cell and incubated for 5 minutes to allow MTs to bind to the kinesin coated surface. The flow cell was washed with motility solution to remove any unbound MTs. sQDs were diluted to a final concentration of 10 nM in motility solution as described above except substituting 1 mM ATP for AMP-PNP to facilitate MT mobility, and supplementing with 1 mM Trolox to optimize photoprotection.[48] The sQD solution was added to the flow chamber and incubated for 5 min to allow sufficient sQD attachment to the biotinylated MT domains, followed by several wash steps using motility solution containing ATP to remove excess sQDs.

Fluorescence Microscopy

The flow cells were mounted on an Olympus IX-71 inverted fluorescence microscope equipped with a 100 W mercury fluorescence lamp (Osram) and an ORCA-3CCD digital camera (Hamamatsu). Olympus filter sets U-MWU2 (AMCA), U-MWIB3 (488 fluorophores), and Chroma dual-band filter set U-N51009 (simultaneous visualization of 488 fluorophores and sQD 655) were used. Fluorescence images were acquired using 60× and 100× oil immersion objectives. Image processing and tracking of spool formation were performed in Fiji[49]. Lengths and number of MTs were measured before and after the addition of sQDs using the Neurite Tracing function[50] in Fiji. The area of a spool (A_{spool}) was determined by measuring the overall and inner diameters of a given spool and calculating $A_{spool} = \pi(d_o\text{-}d_i/2)^2$. Statistical analyses and plotting were performed using SigmaPlot 13.0 (Systat Software, San Jose, CA).

Calculation of fraction defect MTs in spools

The expected fraction of non-bonding MTs in spools, F_d, (orange line in Fig. 3) was calculated by the following. The total length of non-bonding MTs expected in the spools $n = f_n \cdot n_s \cdot \overline{l}_s$, where f_n is the fraction non-bonding in segmented MTs, n_s is the number of segmented MTs, and $\overline{l}_s$ is the average length of the segmented MTs. All of these parameters were measured experimentally for each relative non-bonding level (Fig. S2). Similarly, the total length of bonding MTs expected

in spools was $L_b = f_b \cdot n_s \cdot \overline{l}_s + n_b \cdot \overline{l}_b$, where f_b is the fraction bonding in segmented spools (f_b=1-f_n), n_b is the number of bonding MTs, and $\overline{l}_b$ is the average length of bonding MTs. Then the fraction non-bonding in spools was estimated by $f_n = l_n/(l_n + l_b)$. At low non-bonding MT levels, almost all the non-bonding MTs are in segmented MTs, with very few purely non-bonding MTs. At higher relative non-bonding levels, more of non-bonding domains are in pure non-bonding MTs and fewer are in segmented MTs. For the green line in Fig. 3, the ratio of green (non-bonding) to red (bonding) fluorescence intensity in the spools was calculated for each of the different levels of non-bonding domains. Images were split into separate color channels (red/green). After background subtraction, a standard curve was generated from the intensity ratios and fraction of non-bonding MTs by length. The ratio of bonding (red) and non-bonding (green) MTs in spools was calculated based on this standard curve.

Conflicts of interest

There are no conflicts to declare.

Acknowledgements

Notes and references

1   D. R. Askeland, P. P. Fulay and W. J. Wright, *The Science and Engineering of Materials,* Cengage Learning, Stamford, CT, 6th edn., 2011.

2   H. J. Queisser and E. E. Haller, *Science*, 1998, **281**, 945.

3   C. Sun, R. Hui and J. Roller, *J. Solid State Electrochem.*, 2010, **14**, 1125.

4   P. Szuromi and D. Clery, *Science*, 1998, **281**, 939.

5   J. William D. Callister and David G. Rethwisch, *Materials Science and Engineering*, John Wiley & Sons, Inc., Hoboken, NJ, 9th edn., 2014.

6   M. D. Hager, P. Greil, C. Leyens, S. Van Der Zwaag and U. S. Schubert, *Adv. Mater.*, 2010, **22**, 5424.

7   D. G. Greenhalgh, *Int. J. Biochem. Cell Biol.*, 1998, 30, 1019.

8   Y. C. Yuan, T. Yin, M. Z. Rong and M. Q. Zhang, *Express Polym. Lett.*, 2008, **2**, 238.

9   J. Li, O. E. Shklyaev, T. Li, W. Liu, H. Shum, I. Rozen, A. C. Balazs and J. Wang, *Nano Lett.*, 2015, **15**, 7077.

10   G. D. Bachand, N. F. Bouxsein, V. VanDelinder and M. Bachand, *Wiley Interdiscip. Rev. Nanomed. Nanobiotechnol.*, 2014, **6**, 163.

11   S. M. Block, *Cell*, 1998, **93**, 5–8.

12   R. D. Vale and R. A. Milligan, *Science*, 2000, **288**, 88.

13   K. J. Böhm, *Cell Biol. Int.*, 2008, **32**, 588.

14   H. Hess, V. Vogel, H. H. U and V. Vogel, *Rev. Mol. Biotechnol.*, 2001, **82**, 67.

15   B. M. Mulder and M. E. Janson, *Nat. Mater.*, 2015, **14**, 1080.

16   J. Boekhoven, W. E. Hendriksen, G. J. M. Koper, R. Eelkema and J. H. Van Esch, *Science*, 2015, **349**, 1075.

17   J. Palacci, S. Sacanna, A. Abramian, J. Barral, K. Hanson, A. Y. Grosberg, D. J. Pine and P. M. Chaikin, *Sci. Adv.*, 2015, **1**, e1400214.

18   J. Wang and K. M. Manesh, *Small*, 2010, **6**, 338.

19   S. Sanchez, L. Soler and J. Katuri, *Angew. Chemie - Int. Ed.*, 2015, **54**, 1414.

20   J. Wang, *ACS Nano*, 2009, **3**, 4.

21   K. Kim, J. Guo, X. Xu and D. L. Fan, *Small*, 2015, **11**, 4037.

22   M. Ibele, T. E. Mallouk and A. Sen, *Angew. Chemie - Int. Ed.*, 2009, **48**, 3308.

23   G. D. Bachand, H. Hess, B. Ratna, P. Satir and V. Vogel, *Lab Chip*, 2009, **9**, 1661.

24   T. Korten, A. Mansson, S. Diez, A. Månsson and S. Diez, *Curr. Opin. Biotechnol.*, 2010, **21**, 477.

25   H. Hess and J. L. Ross, *Chem. Soc. Rev.*, 2017, **46**, 5570.

26   T. Fischer, A. Agarwal and H. Hess, *Nat. Nanotechnol.*, 2009, **4**, 162.

27   A. M. R. Kabir and A. Kakugo, *Polym. J.*, 2018, **50**, 1139

28   A. T. Lam, V. VanDelinder, A. M. R. Kabir, H. Hess, G. D. Bachand and A. Kakugo, *Soft Matter*, 2016, **12**, 988.

29   L. Schaedel, K. John, J. Gaillard, M. V Nachury, L. Blanchoin and M. Thery, *Nat. Mater.*, 2015, **14**, 1156.

30   R. A. Cross, *Curr. Opin. Cell Biol.*, 2019, **56**, 88.

31   M. Bachand, N. F. Bouxsein, S. Cheng, S. J. Von Hoyningen-Huene, M. J. Stevens and G. D. Bachand, *RSC Adv.*, 2014, **4**, 54641.

32   V. VanDelinder, S. Brener and G. D. Bachand, *Biomacromolecules*, 2016, **17**, 1048.

33   M. Bachand, A. M. Trent, B. C. Bunker and G. D. Bachand, *J. Nanosci. Nanotechnol.*, 2005, **5**, 718.

34   H. Hess, J. Clemmens, C. Brunner, R. Doot, S. Luna, K. H. Ernst and V. Vogel, *Nano Lett.*, 2005, **5**, 629.

35   H. Hess and G. D. Bachand, *Mater. Today*, 2005, **8**, 22.

36   S. Chaudhuri, T. Korten, S. Korten, G. Milani, T. Lana, G., Te Kronnie and S. Diez, *Nano Lett.*, 2017, **18**, 117.

37   H. Liu and G. D. Bachand, *Cell. Mol. Bioeng.*, 2013, **6**, 98.

38   H. Q. Liu, E. D. Spoerke, M. Bachand, S. J. Koch,. B. C. Bunker and G. D. Bachand, *Adv. Mater.*, 2008, **20**, 4476.

39   H. Kaur, S. Kumar, D. Kukkar, I. Kaur, K. Singh and L. M. Bharadwaj, *J. Biomed. Nanotechnol.*, 2010, **6**, 279.

40   H. Liu and G. D. Bachand, *Soft Matter*, 2011, **7**, 3087.

41   A. C. Greene, M. Bachand, A. Gomez, M. J. Stevens and G. D. Bachand, *Chem. Commun.*, 2017, **53**, 4493.

42   R. C. Williams and L. a. Rone, *Protoplasma*, 1988, **145**, 200.

43   S. Wada, A. M. Kabir, R. Kawamura, M. Ito, D. Inoue, K. Sada and A. Kakugo, *Biomacromolecules*, 2015, **16**, 374.

44   R. Kawamura, A. Kakugo, K. Shikinaka, Y. Osada and J. P. Gong, *Biomacromolecules*, 2008, **9**, 2277.

45   D. Inoue, A. M. R. Kabir, H. Mayama, J. P. Gong, K. Sada and A. Kakugo, *Soft Matter*, 2013, **9**, 7061.

46   C. M. Waterman-Storer and E. D. Salmon, *J. Cell Biol.*, 1997, **139**, 417.

47   D. L. Coy, M. Wagenbach and J. Howard, *J. Biol. Chem.*, 1999, **274**, 3667.

48   V. VanDelinder and G. D. Bachand, *Anal. Chem.*, 2014, **86**, 721.

49   J. Schindelin, I. Arganda-Carreras, E. Frise, V. Kaynig, M. Longair, T. Pietzsch, S. Preibisch, C. Rueden, S. Saalfeld, B. Schmid, J.-Y. Tinevez, D. J. White, V. Hartenstein, K. Liceiri, P. Tomancak and A. Cardona, *Nat. Methods*, 2012, **9**, 676.

50   M. H. Longair, D. A. Baker and J. D. Armstrong, *Bioinformatics*, 2011, **27**, 2453.

TOC Image
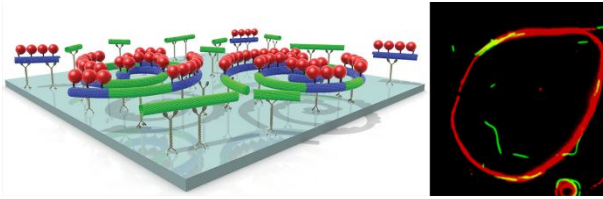
We describe the autonomous removal of non-bonding domains during motor-driven assembly of microtubule spools.